nature structural & molecular biology

A cancer-associated BRCA2 mutation reveals masked nuclear export signals controlling localization

Anand D Jeyasekharan[1], Yang Liu[1], Hiroyoshi Hattori[1,3], Venkat Pisupati[1,3], Asta Bjork Jonsdottir[1], Eeson Rajendra[1], Miyoung Lee[1], Elayanambi Sundaramoorthy[1], Simon Schlachter[2], Clemens F Kaminski[2], Yaara Rosenfeld[1], Ko Sato[1], Jane Savill[1], Nabieh Ayoub[1] & Ashok R Venkitaraman[1]

Germline missense mutations affecting a single *BRCA2* allele predispose humans to cancer. Here we identify a protein-targeting mechanism that is disrupted by the cancer-associated mutation, *BRCA2*^{D2723H}, and that controls the nuclear localization of BRCA2 and its cargo, the recombination enzyme RAD51. A nuclear export signal (NES) in BRCA2 is masked by its interaction with a partner protein, DSS1, such that point mutations impairing BRCA2-DSS1 binding render BRCA2 cytoplasmic. In turn, cytoplasmic mislocalization of mutant BRCA2 inhibits the nuclear retention of RAD51 by exposing a similar NES in RAD51 that is usually obscured by the BRCA2-RAD51 interaction. Thus, a series of NES-masking interactions localizes BRCA2 and RAD51 in the nucleus. Notably, BRCA2^{D2723H} decreases RAD51 nuclear retention even when wild-type BRCA2 is also present. Our findings suggest a mechanism for the regulation of the nucleocytoplasmic distribution of BRCA2 and RAD51 and its impairment by a heterozygous disease-associated mutation.

Inherited germline mutations in a single copy of the *BRCA2* tumor-suppressor gene predispose to breast, ovarian, pancreatic and other cancers[1]. Somatic loss of the second allele may occur in tumors that develop in mutation carriers[2,3], as with other tumor-suppressor genes[4], but loss of this second allele is not always essential for tumorigenesis[5]. Much evidence has suggested that BRCA2 exerts its tumor-suppressive function in the cell nucleus through its role in the repair of DNA breaks by homologous recombination (HR)[6,7]. BRCA2 controls the accumulation of the RAD51 recombinase enzyme at sites of DNA breakage in the nucleus[8,9], nucleates RAD51 filament formation at single-stranded DNA (ssDNA)–double-stranded DNA (dsDNA) junctions[10] and promotes RAD51 binding on ssDNA while inhibiting dsDNA binding[11–15]. However, defective HR typically occurs in cells lacking both *BRCA2* alleles[7], and so it remains unclear how heterozygous cancer-associated mutations may compromise the function of BRCA2.

To address this issue, we investigated the cellular effects of a common cancer-associated *BRCA2* missense mutation (BRCA2^{D2723H}) in which Asp2723 is replaced by histidine[16]. Remarkably, our studies reveal an unreported mechanism wherein the localization of BRCA2 and RAD51 to the cell nucleus is governed by the masking of NESs by protein-protein interactions. The BRCA2^{D2723H} mutant impairs this mechanism, triggering decreased nuclear accumulation of RAD51 even when wild-type (WT) BRCA2 is also present, which contributes to its deleterious effects in the heterozygous state. Thus, our results link the nucleocytoplasmic translocation of the BRCA2 tumor suppressor to the cellular mechanisms of disease after its germline inactivation.

RESULTS

DSS1 binding to BRCA2 is critical for nuclear localization

Cancer-associated missense mutations in human BRCA2 occur frequently in the region that spans residues ~2500–2850 (ref. 17), which mediates the interaction (**Supplementary Fig. 1a**) of BRCA2 with the small (70-residue), acidic protein DSS1 (refs. 18,19). One of these mutations, BRCA2^{D2723H}, which alters a single aspartic acid residue at position 2723 in the 3418-residue BRCA2 protein to histidine, has been reported >30 times in the Breast Cancer Information Core database (http://research.nhgri.nih.gov/bic/). Evidence from linkage analysis of human kindreds[16] and functional studies on mouse embryonic stem (ES) cells has suggested that the inheritance of BRCA2^{D2723H} is functionally deleterious[20]. Because the BRCA2^{D2723H} mutation affects a key conserved residue (**Supplementary Fig. 1a**) that directly contacts DSS1 (ref. 19), we first determined whether it affects the BRCA2-DSS1 interaction. We generated a fragment of BRCA2 spanning the entire DSS1-binding domain (DBD) across residues 2461–2975 fused to 'super' YFP (sYFP) plus a nuclear localization signal (NLS) and coexpressed it in human 293T cells with an mCherry-tagged form of full-length DSS1. The sYFP-DBD fragment is >70 kDa long and therefore requires a heterologous NLS to induce nuclear localization. Although the WT form of NLS-sYFP-DBD coimmunoprecipitated with mCherry-DSS1 (**Fig. 1a**), the BRCA2^{D2723H} mutant did not, despite having higher expression levels. Similarly, a mutant form of the DBD (BRCA2^{W2725A}) in which an evolutionarily conserved tryptophan residue at position 2725 that has been implicated in DSS1 binding[21] is altered to alanine immunoprecipitated poorly with mCherry-DSS1.

[1]The Medical Research Council (MRC) Cancer Unit, University of Cambridge, Hutchison–MRC Research Centre, Cambridge, UK. [2]Department of Chemical Engineering, University of Cambridge, Cambridge, UK. [3]These authors contributed equally to this work. Correspondence should be addressed to A.R.V. (arv22@cam.ac.uk).

Received 6 May; accepted 25 July; published online 8 September 2013; doi:10.1038/nsmb.2666

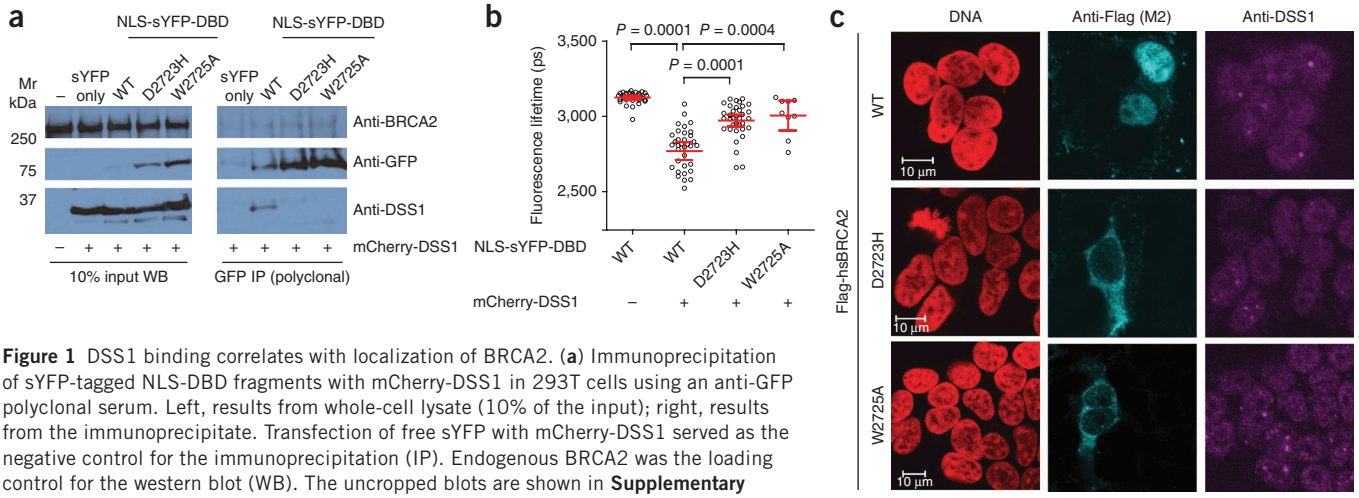

Figure 1 DSS1 binding correlates with localization of BRCA2. (**a**) Immunoprecipitation of sYFP-tagged NLS-DBD fragments with mCherry-DSS1 in 293T cells using an anti-GFP polyclonal serum. Left, results from whole-cell lysate (10% of the input); right, results from the immunoprecipitate. Transfection of free sYFP with mCherry-DSS1 served as the negative control for the immunoprecipitation (IP). Endogenous BRCA2 was the loading control for the western blot (WB). The uncropped blots are shown in **Supplementary Figure 8**. Mr, relative molecular weight. (**b**) Dot plot of the mean sYFP lifetime per cell from a FRET-FLIM experiment with NLS-sYFP-DBD and mCherry-DSS1. Each dot represents a single cell; the horizontal lines and error bars represent the means and 95% confidence intervals, respectively, for the population studied in the experiment. U2OS cells co-transfected with the indicated constructs were analyzed by TCSPC. The *P* values shown were calculated by two-tailed Student's *t* test. $n = 35$ cells for WT, WT + DSS1 and D2723H + DSS1; $n - 9$ cells for W2725A + DSS1. (**c**) Representative immunofluorescent confocal micrographs of 293T cells nucleofected with Flag-tagged full-length versions of human (hs) WT BRCA2, BRCA2^{D2723H} or BRCA2^{W2725A}. Red indicates DNA, cyan indicates BRCA2 (detected by anti-Flag) and purple indicates endogenous DSS1 (detected by anti-DSS1).

Measurement of fluorescence resonance energy transfer (FRET) (**Supplementary Fig. 1b**), a near-field coupling effect, reports on specific intermolecular interactions when the interacting fluorophores are less than ~5 nm apart[22]. sYFP and mCherry are an optimized FRET pair, with a Förster radius of >5 nm, and thus exhibit an enhanced FRET efficiency compared to traditional blue-shifted fluorophore pairs[23]. We used fluorescence lifetime imaging microscopy (FLIM) to measure FRET on the donor sYFP molecule, which has a fluorescence lifetime that shows monoexponential decay[23] (**Supplementary Fig. 1c**). Co-transfection of mCherry-DSS1 with NLS-sYFP-DBD caused a significant decrease in the lifetime of sYFP from 3,100 to 2,750 ps on average, as evidenced by time-correlated single photon counting (TCSPC), which is suggestive of FRET through the direct interaction of these molecules (**Fig. 1b** and **Supplementary Fig. 1d**). In contrast, the lifetime of the NLS-sYFP–tagged BRCA2^{D2723H} and BRCA2^{W2725A} mutants remained close to 3,000 ps, confirming that the mutations inhibit the interaction of the BRCA2 DBD with DSS1 directly (**Fig. 1b**). Human BRCA2 normally localizes to the cell nucleus through tandem nuclear localization signals (NLSs) at its extreme C terminus[24]. In contrast, full-length BRCA2 harboring the D2723H mutation mislocalized predominantly to the cytoplasm in transfected cells (**Fig. 1c**), as has been shown previously[20,25]. Notably, BRCA2^{W2725A} similarly mislocalized (**Fig. 1c**), suggesting a correlation between the loss of DSS1 binding and cytoplasmic mislocalization.

DSS1 masks a nuclear exclusion sequence in BRCA2

Neither the D2723H nor the W2725A mutation is predicted to alter the canonical NLSs positioned in exon 27 of BRCA2 (ref. 24). This prompted us to survey BRCA2 for NESs using the NetNES algorithm, which employs neural networks to predict consensus motifs fitting the pattern $\phi X_{1-3}\phi X_{1-3}\phi X\phi$, where ϕ is a hydrophobic amino acid (methionine, phenylalanine, isoleucine, valine or leucine) and X is any amino acid[26]. We detected four such potential NES motifs in the DSS1-binding region of BRCA2 (**Supplementary Fig. 2a**). One motif (residues 2682–2698, encoded in exon 18 of *BRCA2*) showed strong evolutionary conservation, particularly of the critical hydrophobic residues (**Fig. 2a**). When fused to sYFP, this motif induced nuclear exclusion, which is in contrast to the effects of a control BRCA2-derived peptide of similar size (**Fig. 2b**); these results substantiate the NES function of the motif.

The cytoplasmic mislocalization of BRCA2 mutants carrying alterations that affect DSS1 binding, but not intrinsic NLS or NES motifs, raises the possibility that the BRCA2-DSS1 interaction masks an NES of BRCA2. Consistent with this idea, the structure of the BRCA2-DSS1 complex[19] suggests that the residues that are critical for binding to exportins in the potential NES spanning residues 2682–2698 in BRCA2 are obscured by DSS1 (**Fig. 2c**). Moreover, overexpression of DSS1 in cells expressing WT forms of either NLS-sYFP-DBD or full-length BRCA2 enhanced nuclear localization, whereas the BRCA2^{D2723H} and BRCA2^{W2725A} mutants were not similarly affected (**Supplementary Fig. 2b–d**). Together these findings support a model wherein the binding of DSS1 to BRCA2 is essential for its nuclear retention through the masking of an NES within the DBD.

BRCA2 masks a nuclear exclusion sequence in RAD51

The RAD51 recombinase, a 37-kDa protein that is central to DNA repair by HR[27], binds directly to the BRC repeats of BRCA2 (refs. 6,28), creating an interaction that is essential for the efficient completion of recombination reactions[10–14]. Eight BRC repeats are present in human BRCA2, and the structural basis of their interaction with RAD51 has been characterized by crystallography and structure-function analyses in mammalian cells[28,29]. Notably, a NetNES analysis of human RAD51 identified a putative NES spanning residues 245–260 (**Fig. 3a**) that is strongly conserved across species (**Fig. 3b**). This NES lies within a recently identified binding site for the BRC repeats of BRCA2 (ref. 29), and an examination of the crystal structure revealed that key exportin-binding residues within this RAD51 NES are probably masked when the protein is bound to BRCA2 (**Fig. 3c**). The RAD51 NES was sufficient to exclude sYFP from the nucleus when fused to the fluorophore (**Fig. 3d**). Mutation of the residues Ser208 and Ala209 in RAD51 has been reported to abolish its binding to the BRC repeats in BRCA2 but not its ability to oligomerize[30].

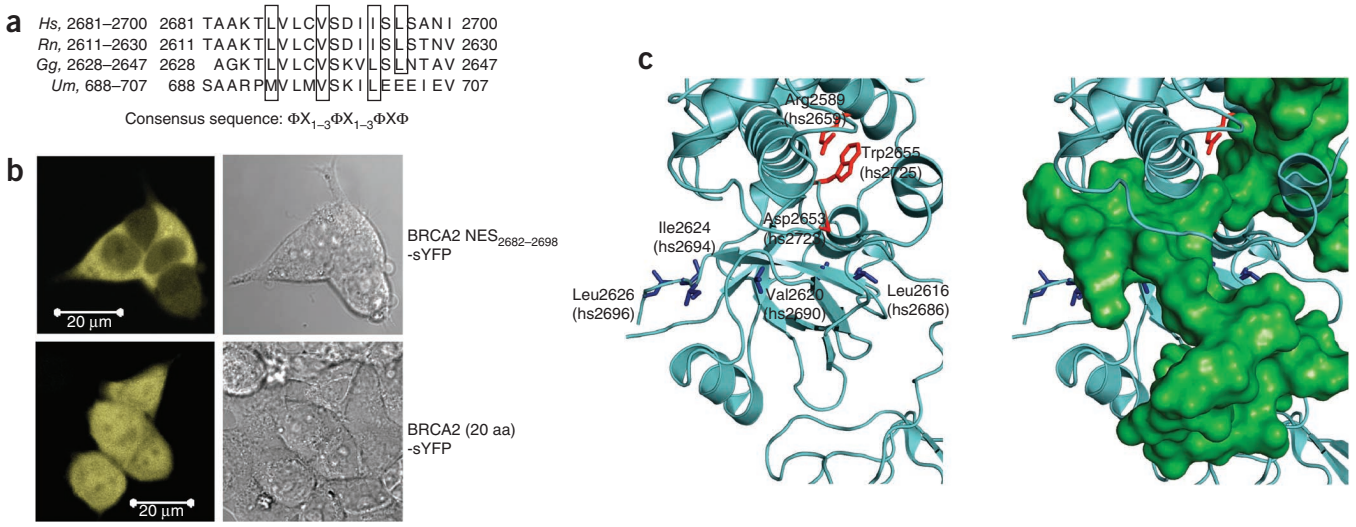

Figure 2 DSS1 regulates a functional NES in BRCA2. (**a**) ClustalW alignment of the nuclear exclusion signal within the DBD of BRCA2, with the critical hydrophobic residues that potentially contribute to the NES consensus indicated by black boxes. *Hs*, *Homo sapiens*; *Rn*, *Rattus norvegicus*; *Gg*, *Gallus gallus*; *Um*, *U. maydis*. The numbers to the right of the species abbreviations indicate the residues shown. (**b**) A representative fluorescent micrograph (of three total replicates) of 293T cells transfected with a BRCA2 NES-sYFP construct (top) or sYFP tagged to a similarly sized sequence within BRCA2 (bottom), which served as a negative control. aa, amino acids. (**c**) A rendering of the structure of rat (rn) BRCA2 DBD (PDB 1IYJ), with homologous human (hs) residues indiated underneath. The critical hydrophobic NES residues are highlighted in dark blue[10] and mutations that affect DSS1 binding are depicted in red. On the right is a superimposition of DSS1 (green).

This mutant localized to the cytoplasm when expressed in DT40 cells lacking endogenous RAD51 (**Fig. 3e**). These observations not only confirm that the nuclear retention of RAD51 requires binding to BRCA2 but also corroborate that a RAD51 NES is masked by interaction with the BRC repeats of BRCA2.

In vitro interaction of CRM1 with NESs in BRCA2 and RAD51

We demonstrated that putative NESs identified in the DSS1-binding domain of BRCA2 and the BRCA2-binding region of RAD51 share the expected consensus characteristics and can direct the nuclear exclusion of sYFP when fused to this heterologous protein. However, leucine residues in NES-like motifs frequently contribute to the buried hydrophobic cores of protein folds and may therefore be inaccessible for interaction with the nuclear exportin CRM1 in their native context[31,32]. To address this issue, we tested the ability of glutathione S-transferase (GST)-tagged forms of the NES-containing domains of BRCA2 and RAD51 to bind *in vitro* to recombinant CRM1 in the presence of an active GTP-bound Q69L form of the essential cofactor Ran under the experimental conditions described previously[33]. We found that a GST-tagged recombinant protein encoding the DBD region of BRCA2 bound to recombinant CRM1 in the presence of

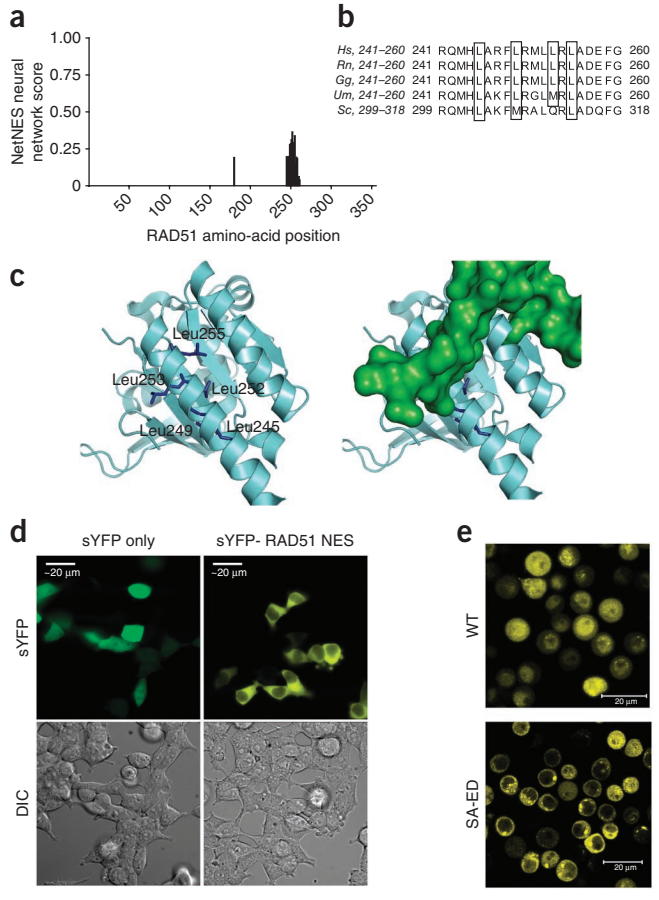

Figure 3 BRCA2 regulates a functional NES in RAD51. (**a**) NES scores for amino acids in the hsRAD51 sequence, as determined by the NetNES algorithm, showing the potential NES sequence in the C terminus of the protein. (**b**) Sequence alignment of the residues comprising the RAD51 NES from yeast (*S. cerevisiae*, *Sc*) to human. The hydrophobic residues are indicated by black boxes. (**c**) Rendering of RAD51-BRCA2 (PDB 1N0W)[28] using the same color scheme as in **Fig. 2c**. NES residues in RAD51 are shown in dark blue. On the right is a superimposition of the bound BRC repeat (green). (**d**) Representative micrographs (of two total replicates) of 293T cells transfected with a RAD51-NES–tagged version of sYFP (right) in comparison to free sYFP alone (left). DIC, differential interference contrast. (**e**) Fluorescence micrograph (representative of two total replicates) of sYFP-tagged human WT RAD51 compared with a mutant form of the protein that lacks BRCA2 binding (sYFP-RAD51 (SA-ED)). sYFP-tagged human proteins were expressed in *RAD51*$^{-/-}$ DT40 cells that conditionally expressed tetracycline (Tet)-regulated untagged RAD51. Micrographs were taken 12 h after the depletion of untagged RAD51 using doxycycline[30].

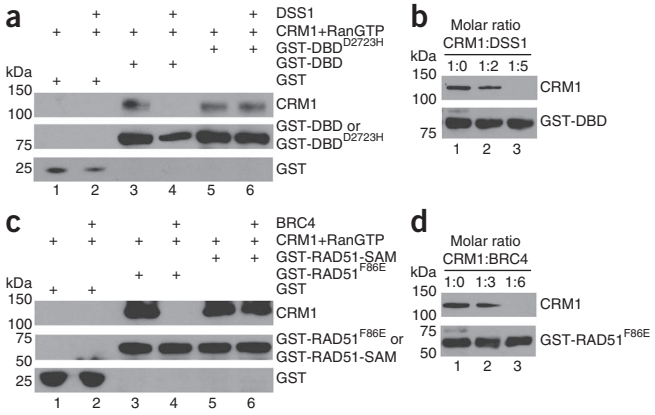

Figure 4 CRM1 binding to NESs in BRCA2 or RAD51 is masked by DSS1 or BRC4, respectively. (**a**) Immunoblots of GST pulldown assays assessing the binding of CRM1 to GST-DBD (lanes 3 and 4) and GST-DBD^{D2723H} (lanes 5 and 6) immobilized on a glutathione-Sepharose matrix in the absence (lanes 3 and 5) or presence (lanes 4 and 6) of DSS1 at a five-fold molar excess. (**b**) Representative titration (of three total replicates) with GST as a specificity control, from which the molar excess of DSS1 used in **a** was optimized. (**c**) Immunoblots of GST pulldown assays assessing binding of CRM1 to GST-RAD51^{F86E} (lanes 3 and 4) and GST-RAD51-SAM (lanes 5 and 6) immobilized on a glutathione-Sepharose matrix in the absence (lanes 3 and 5) or presence of (lanes 4 and 6) of BRC4 peptide at a six-fold molar excess. (**d**) Representative titration (of three total replicates) with GST as a specificity control, from which the molar excess of BRC4 peptide used in **c** was optimized. Proteins were visualized with antibodies to histidine or GST. CRM1 protein was tagged with histidine (uncropped blots are shown in **Supplementary Fig. 8**).

Ran-GTP (**Fig. 4a**, lane 3), whereas GST alone did not (**Fig. 4a**, lane 1). Moreover, the addition of DSS1 inhibited this interaction (**Fig. 4a**, lane 4) in a dose-dependent manner (**Fig. 4b**). These results prompted us to test the effect of the D2723H mutation, which is expected to prevent DSS1 binding. Indeed, the D2723H mutant form of the BRCA2 DBD interacted constitutively with CRM1 regardless of whether DSS1 was present (**Fig. 4a**, lanes 5 and 6). Thus, our findings provide biochemical evidence that the DBD region of BRCA2 contains authentic NES motifs that are capable of binding CRM1, that this interaction is lost when the NESs are masked by the binding of DSS1 and that loss of this interaction in the BRCA2^{D2723H} mutant promotes constitutive CRM1 binding, which is consistent with the nuclear export and cytoplasmic mislocalization of the mutant protein.

In addition, we found biochemical evidence that RAD51 contains CRM1-binding NESs that are masked by interaction with the BRC4 region of BRCA2. In these experiments, we used the F86E form of RAD51, which we characterized previously[28,30], to enable its purification without the spontaneous *in vitro* aggregation that is typical of recombinant WT RAD51 (refs. 28,34). A GST-tagged version of this protein bound to CRM1 in the presence of Ran-GTP (**Fig. 4c**). The addition of the BRC4 region of BRCA2 prevented CRM1 binding (**Fig. 4c**, compare lanes 3 and 4) in a dose-dependent manner (**Fig. 4d**). Notably, a mutant form of RAD51 (SAM208-210LEA, denoted here RAD51-SAM), which we have previously shown[28,30] to be incapable of BRC4 binding, interacted constitutively with CRM1 regardless of whether BRC4 was present (**Fig. 4d**, lanes 5 and 6). Thus, these *in vitro*

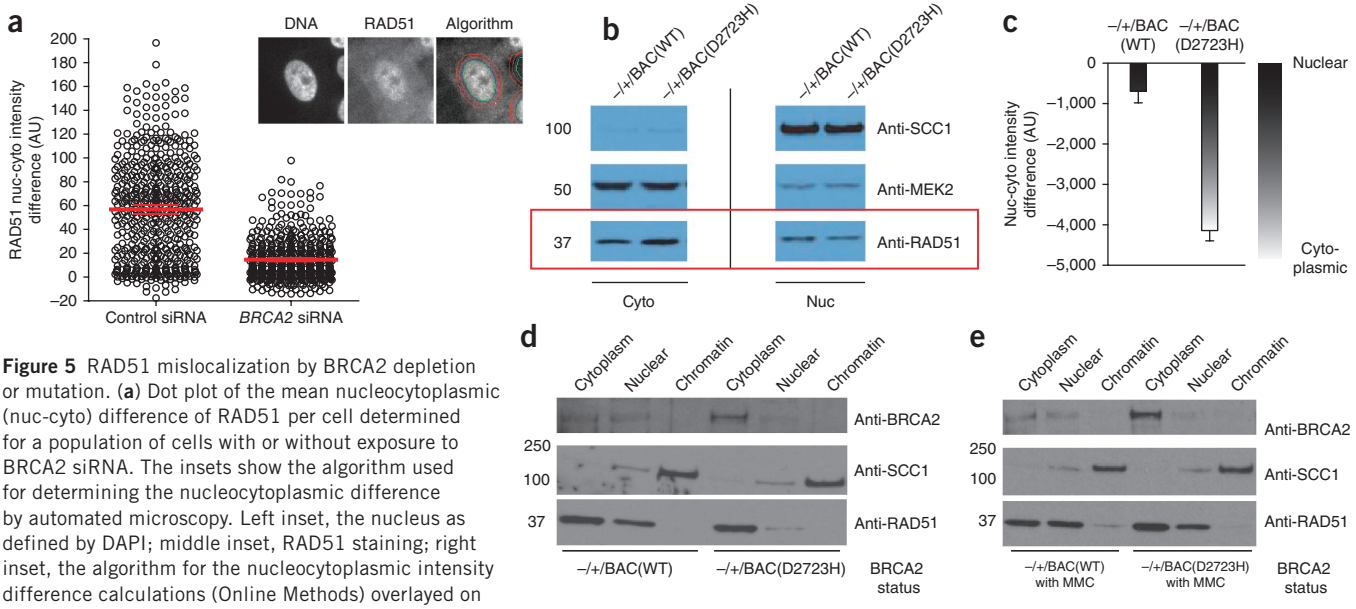

Figure 5 RAD51 mislocalization by BRCA2 depletion or mutation. (**a**) Dot plot of the mean nucleocytoplasmic (nuc-cyto) difference of RAD51 per cell determined for a population of cells with or without exposure to BRCA2 siRNA. The insets show the algorithm used for determining the nucleocytoplasmic difference by automated microscopy. Left inset, the nucleus as defined by DAPI; middle inset, RAD51 staining; right inset, the algorithm for the nucleocytoplasmic intensity difference calculations (Online Methods) overlayed on the RAD51 image. AU, arbitrary units. Each circle represents the value from a single cell, the red lines indicate the means, and the error bars represent the 95% confidence intervals. n = 2,554 cells (control) or n = 2,478 cells (siBRCA2). (**b**) Cell fractionation experiment results from heterozygous mouse ES cells with western blotting for RAD51 to assess localization. MEK2 (which is predominantly cytoplasmic (cyto)) and SCC1 (which is predominantly nuclear (nuc)) served as loading controls as well as controls for the efficiency of fractionation. BAC(WT) indicates cells carrying a BAC expressing WT BRCA2; BAC(D2723H) indicates cells carrying a BAC expressing BRCA2^{D2723H}. (**c**) Bar graph quantifying the results from three independent fractionation experiments. The nucleocytoplasmic intensity difference for RAD51 in each experiment was obtained by generating densitometric profiles for each band (identical exposure) using ImageJ and then subtracting the cytoplasmic value from the nuclear value. Lower (more negative) values indicate more cytoplasmic protein (n = 3 independent fractionation experiments; error bars, s.e.m.). (**d**,**e**) Cell fractionation experiment results from ES cells carrying BACs expressing either WT BRCA2 or BRCA2^{D2723H} in the absence (**d**) or presence (**e**) of DNA damage induced by exposure to 100 ng ml^{-1} of MMC for 20 h. SCC1 was used as a control for fractionation. One experiment representative of three independent repeats is shown. Uncropped blots are shown in **Supplementary Figure 8**.

results recapitulating exportin-cargo interactions using recombinant proteins provided strong biochemical evidence for a model wherein CRM1-dependent nuclear export—and its masking by protein-protein interactions—is a critical determinant of BRCA2 and RAD51 localization.

Our attempt at *en bloc* replacement of consensus hydrophobic residues within the proposed NESs (by substitution with alanine of Leu2686, Leu2688, Leu2696 and Ile2694 in the BRCA2 stretch from residues 2682–2698 and of Leu245, Leu249, Leu253 and Leu255 in the RAD51 stretch from residues 245–260) was beyond the scope of this work, as the BRCA2 and RAD51 domains encoding the putative NESs exhibited poor yield and solubility in bacterial expression. Moreover, further mutational analysis of the contributions made by residues located outside these motifs is difficult because the exact length and nature of the NES sequences that are required for CRM1 binding have been reported to be variable[33,35], as are the potential binding modes between CRM1 and its various substrates[36]. Future structural work will be required to precisely define the residues contributing to NES activity.

A heterozygous D2723H mutation in BRCA2 mislocalizes RAD51

Our findings suggest that the nuclear retention of BRCA2 and RAD51 depends on NES-masking interactions between BRCA2 and DSS1 and between BRCA2 and RAD51. To investigate whether these interactions are interdependent, we first tested the effect of BRCA2 depletion on RAD51 localization using RNA interference (**Fig. 5a**). We used an automated microscopic assay in which the nucleocytoplasmic difference is calculated by subtracting the amount of RAD51 in a cytoplasmic ring surrounding the nucleus from the amount of RAD51 in a circular area within the nuclear boundary (as defined by DNA staining) (**Fig. 5a**, inset). We found that depletion of BRCA2 by RNA interference decreased the nuclear localization of RAD51 (**Fig. 5a** and **Supplementary Fig. 3a–c**), which is consistent with a role for BRCA2 in the nuclear retention of RAD51.

Because humans who inherit the D2723H mutation on a single allele of *BRCA2* are predisposed to cancer, this raises the possibility that the mutant protein exerts a *trans*-dominant effect on RAD51 localization when in the heterozygous state. Accordingly, we examined RAD51 localization in mouse ES cells engineered to be heterozygous for the human BRCA2^{D2723H} mutant in comparison to an appropriate WT control in an identical genetic background[20]. In this system, one allele of mouse (mm) *Brca2* was disrupted by gene targeting, and the cells were complemented with a bacterial artificial chromosome (BAC) containing a segment of human chromosome 13 encoding human (hs) BRCA2. This BAC has been reported to drive near-endogenous expression of BRCA2 and is sufficient to replace mmBrca2 function in these cells, as evidenced by the rescue of lethality when the second endogenous mm*Brca2* allele is also disrupted[20]. The total levels of BRCA2 and RAD51 expression were comparable in ES cells expressing either WT BRCA2 or BRCA2^{D2723H} (**Supplementary Fig. 4a,b**). We examined the distribution of RAD51 in these cells by biochemical fractionation and quantitative western blotting (**Fig. 5b**) because of technical difficulties in performing accurate microscopic analyses of protein localization in the ES cells. We observed an increase in the amount of cytoplasmic RAD51 in cells carrying a single allele of BRCA2^{D2723H}, with a corresponding decrease in the nuclear levels of the protein (**Fig. 5b,c**) both in the absence (**Fig. 5d**) and presence (**Fig. 5e**) of DNA damage induced by mitomycin C (MMC). Mutant BRCA2^{D2723H} expressed from the BAC in these cells was also predominantly cytoplasmic, unlike WT BRCA2 (ref. 20) (**Fig. 5d,e**).

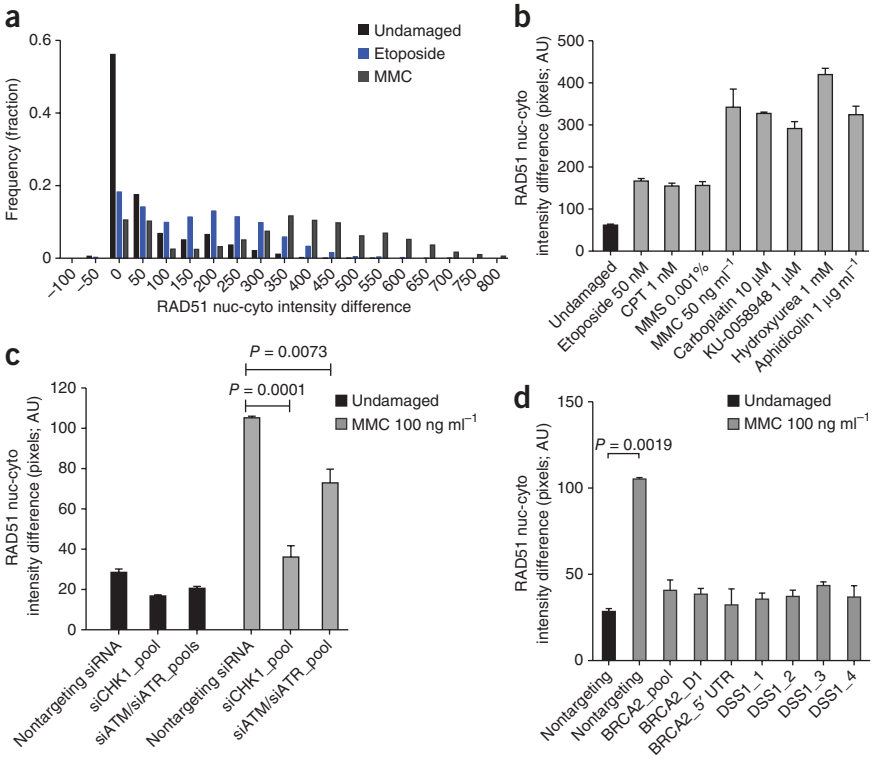

Figure 6 RAD51 nuclear enrichment is a BRCA2-dependent DNA-damage response. (**a**) The frequency distribution of the RAD51 nuclear-cytoplasmic pixel intensity difference (nuc-cyto intensity difference) from different populations of MCF10A cells analyzed by automated immunofluorescence microscopy. $n = 2{,}000$ cells per group. (**b**) The mean nuclear-cytoplasmic intensity difference for RAD51 in MCF10A cells treated with the indicated forms of DNA damage. CPT, camptothecin; MMS, methylmethanesulfonate. Each bar represents the mean ± s.e.m. of 4 wells in a 96-well plate with 500 cells counted per well. (**c**) The mean nuclear-cytoplasmic intensity difference for RAD51 in MCF10A cells pretreated with the indicated siRNAs (siCHK1 is an siRNA targeting CHK1, siATM is an siRNA targeting ATM, siATR is an siRNA targeting ATR, and siATM/siATR indicates treatment with both siATM and siATR) and with (gray) or without (black) exposure to MMC. The increase in the intensity difference after DNA damage was significantly affected (two-tailed Student's *t* test, $n = 500$ cells per well, 3 wells) by depletion of ATM/ATR or CHK1. Error bars, s.e.m. (**d**) The RAD51 nuclear-cytoplasmic intensity difference in MCF10A cells after knockdown of BRCA2 and DSS1 using multiple independent siRNAs (Online Methods). UTR, untranslated region. The black bar on the left represents undamaged cells. The nuclear enrichment after DNA damage was significantly affected (two-tailed Student's *t* test, $n = 500$ cells per well, 3 wells) by depletion of both BRCA2 and DSS1. Error bars, s.e.m. **Supplementary Figure 6a–d** shows the depletion efficiency with the siRNAs used.

Together these findings suggest a mechanism underlying the deleterious effects of the BRCA2^{D2723H} mutant when present in the heterozygous state and coexpressed with WT BRCA2.

BRCA2 and DSS1 promote RAD51 nuclear enrichment

There is evidence that RAD51 is enriched in the nucleus during the response to genotoxic lesions that are repaired by HR[37,38]. We characterized this effect further by analyzing the nucleocytoplasmic distribution of RAD51 after DNA damage in human cells using automated microscopy. Exposure to the DNA-damaging agents etoposide and MMC caused an increase in the relative amount of nuclear RAD51, as evidenced by changes in the nuclear-cytoplasmic difference of the average pixel intensities within the two regions (**Fig. 6a** and **Supplementary Fig. 5**). Moreover, genotoxins (e.g., MMC, carboplatin, the poly-(ADP-ribose) polymerase (PARP) inhibitor KU-0058948, hydroxyurea or aphidicolin) generating DNA lesions that are known to engage pathways for repair by HR enhanced the nuclear enrichment of RAD51 to a greater degree than other genotoxins (**Fig. 6b**). Depletion of ataxia telangiectasia mutated (ATM), ATM and Rad53 related (ATR) or CHK1, which are damage-response kinases[39], diminished the nuclear enrichment of RAD51 after MMC exposure, confirming that this response depends on the cellular pathways that sense and signal DNA damage (**Fig. 6c** and **Supplementary Fig. 6**). Notably, depletion of BRCA2 or DSS1 also affected the nuclear enrichment of RAD51 after genotoxic stress (**Fig. 6d** and **Supplementary Fig. 6**). Using Flag-BRCA2–complemented EUFA423 cells (**Supplementary Fig. 7**), we showed that DNA damage also increases the levels of nuclear BRCA2, as measured with the Cellomics ArrayScan (**Supplementary Fig. 7c**), and depletion of DSS1 causes a decrease in nuclear Flag-BRCA2 levels (**Supplementary Fig. 7d**). Collectively these results suggest that the enhanced nuclear distribution of RAD51 is a DNA-damage response that is dependent on BRCA2 and DSS1 and that may be compromised by cancer-associated mutations that disrupt the DSS1-BRCA2 interaction.

DISCUSSION

The findings we report here suggest a new mechanism controlling the intracellular distribution of the RAD51 recombinase (**Fig. 7**) wherein NESs present in BRCA2 and its cargo, RAD51, must be masked by complex formation between BRCA2, DSS1 and RAD51 in order to permit nuclear localization. The NES-masking mechanism suggested by our findings reveals an additional layer of regulation that has not been recognized in earlier work reporting that RAD51 enters the nucleus only when bound to a partner, RAD51C[38], which contains an NLS.

The location of the proposed NESs near the hydrophobic protein cores (**Figs. 2c** and **3c**) raises the possibility that these motifs are exposed for CRM1 binding by unfolding in the absence of the masking partner protein, suggesting a mechanism to ensure that only functional BRCA2-DSS1-RAD51 complexes are retained in the nucleus. Moreover, RAD51 oligomerization also probably regulates its nuclear localization. Both *in vitro* and *in vivo*[30,34], an equilibrium is believed to exist between RAD51 monomers and oligomers of varying stoichiometries whose abundances are closely regulated by interaction with factors such as RAD52 or the BRC repeats of BRCA2 (refs. 30,40). Although RAD51 monomers (37 kDa) may pass freely into the nucleus, RAD51 oligomers (≥74 kDa) probably do not equilibrate passively across nuclear pores, which generally accommodate substrates ≤60 kDa (reviewed in ref. 41). There is structural[28], biochemical[34] and cell-biological[28,30] evidence that RAD51 oligomerization is suppressed by its interaction with the BRC repeats of BRCA2. This may help create a pool of monomeric RAD51 in the cytoplasm for transport into the nucleus through free nuclear pore entry or for binding to partner proteins (including RAD51C) that contain NLSs. The RAD51 monomer-oligomer equilibrium could also exist within the nucleus but is probably biased toward DNA-bound oligomers or

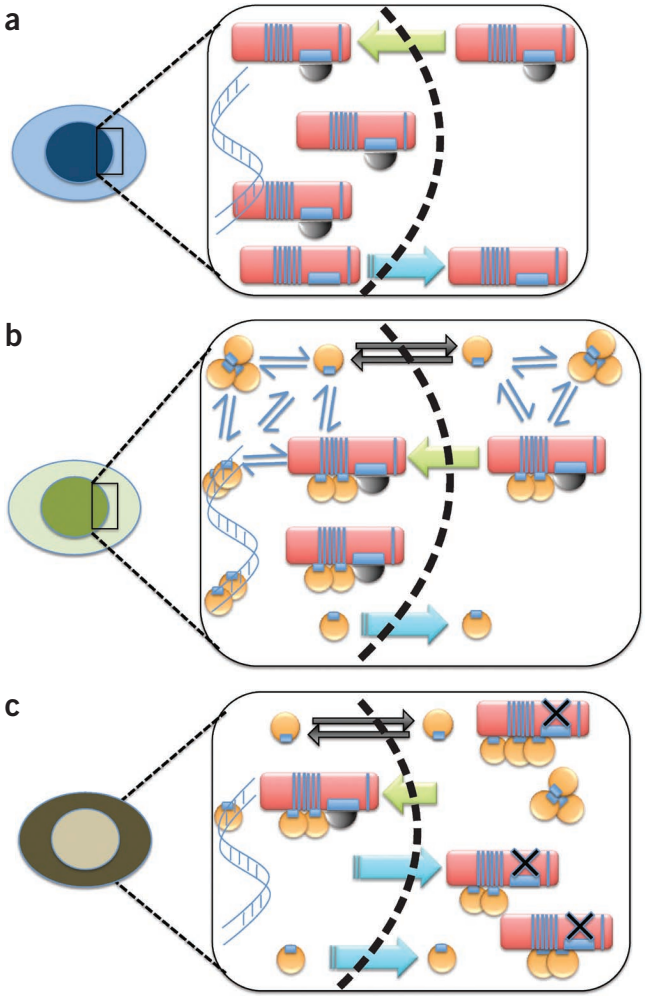

Figure 7 A hypothetical model for BRCA2 and RAD51 nuclear localization through masking of NESs. (**a**) The proposed mechanism wherein the nuclear retention of BRCA2 (red oblong shape) is allowed when its binding to DSS1 (black semicircle) obscures an NES motif. Nuclear transport (green arrow) is presumably directed by NLSs previously identified in the C-terminal region of BRCA2, which are not shown here. Dissociation of BRCA2 from DSS1 may permit nuclear export (blue arrow). (**b**) The proposed mechanism wherein the nuclear retention of RAD51 (orange circle) is allowed when its binding to the BRC repeats of BRCA2 obscures an NES motif. Nuclear transport (green arrow) of the BRCA2-RAD51 complex is presumably directed by the NLSs in BRCA2. In addition, cytosolic RAD51 may exist in an equilibrium (thin blue arrows) between free monomers and oligomers. Monomeric RAD51 is small enough to diffuse freely across the nuclear membrane (black arrows), whereas oligomers are not. Dissociation of RAD51 from BRCA2 may permit nuclear export (blue arrow). The net result of these different processes is to localize RAD51 predominantly in the nucleus. (**c**) How the processes shown in **a** and **b** may be affected by the BRCA2^{D2723H} mutation, which prevents DSS1 binding (black X). Mutant BRCA2 is exported from the nucleus (blue arrows), resulting in predominant cytoplasmic localization, and this is proposed to shift the balance toward cytoplasmic localization of RAD51, despite the presence of WT BRCA2.

monomers in which BRC binding obscures the NES, thus promoting nuclear retention.

Depletion of DSS1, which not only binds to BRCA2 but is also a component of the 19S proteasome[42] and RNA-processing complexes[43], impairs the assembly of RAD51 into foci at sites of DNA damage[44] to mediate DNA HR. This effect has been ascribed previously to a direct function of the BRCA2-DSS1 complex in binding to ssDNA through the formation of oligonucleotide- and oligosaccharide-binding folds[19], which may not only localize RAD51 to these substrates but also displace the ssDNA-binding protein RPA[10]. Our findings suggest an additional function for DSS1 in HR through regulation of the nuclear localization of BRCA2 and, indirectly, RAD51. In this light, it is notable that mutant forms of BRCA2 in which the DSS1 binding domain has been entirely deleted are still capable of supporting HR[45–47]. Moreover, DSS1 is apparently required for HR only when the DBD is present[48]. These observations are consistent with our findings: DBD deletion presumably removes the strong NESs that we identified in this work, obviating the necessity for their masking by DSS1 and allowing mutant forms of BRCA2 lacking the DBD to at least partly function in the nucleus even without DSS1.

We surmise that DBD deletion and loss of DSS1 binding in human BRCA2 may lead to subtle defects in HR, which is reminiscent of the phenotypes observed in mutants of the BRCA2 homolog brh2 in the fungus *Ustilago maydis* that lack dss1 binding[49]. Conversely, the NESs we identified in human BRCA2 are not well conserved in brh2 (**Fig. 2a**), raising the possibility that the mechanisms that regulate BRCA2 nuclear localization are not directly comparable between these species. However, *U. maydis* rad51 contains a conserved NES (**Fig. 3a**), suggesting that its localization may depend on the BRC repeat found in brh2, whereas *Saccharomyces cerevisiae* Rad51 does not (**Fig. 3a**), which is consistent with the absence of a Brca2 homolog in yeast.

Several lines of evidence have suggested that the DSS1-masked NES we identified in BRCA2 is dominant in its function over other motifs such as NLSs within the protein that may control nuclear localization[24,50]. For instance, the BRCA2^{D2723H} and BRCA2^{W2725A} point mutants, which both lack DSS1 binding to mask the NES, mislocalize to the cytosol, and the Brca2^{D2723H} variant is embryonic lethal in mice when homozygous[20], suggesting that it is nonfunctional. Moreover, our findings suggest that these point mutations probably do not exert their effects simply through BRCA2 destabilization, as their protein expression is not markedly decreased. Instead, they speak to a critical role for the DSS1-BRCA2 interaction in the control of BRCA2-RAD51 localization. These findings raise questions regarding the expected clinical effects of the cancer-associated *BRCA2*^{D2723H} allele when expressed in the heterozygous state in germline mutation carriers. Although our findings suggest that *BRCA2*^{D2723H} heterozygosity may suffice to mislocalize RAD51, we are unaware that carriers of this mutation exhibit radiosensitivity or other clinical features that are associated with profound defects in DNA repair, which is consistent with the lack of radiosensitivity of cell lines carrying D2723H *in vitro* (**Supplementary Fig. 4c**). However, patients heterozygous for *BRCA2*^{D2723H} do appear to be at risk of developing early onset cancers, suggesting that this alteration causes a cumulative rather than an acute effect on genome stability, which acts over years to promote carcinogenesis. Indeed, BRCA2 is often cytoplasmic in cancer cells[24], and mislocalization of RAD51 has been reported in both familial breast cancer[51] and sporadic cases of prostate cancer[52].

Notably, our findings also indicate that alterations in the normal intracellular distribution of RAD51 may mark defects in the cellular response to DNA damage arising at several distinct steps (**Fig. 6c**,**d**). We therefore suggest that quantitative measurement of the nucleocytoplasmic levels of RAD51 may serve as a surrogate marker for these defects, which may be of value in assessments of cancer diagnosis or therapeutic responsiveness.

METHODS

Methods and any associated references are available in the online version of the paper.

Note: Any Supplementary Information and Source Data files are available in the online version of the paper.

ACKNOWLEDGMENTS

We acknowledge the generous gifts of WT and BRCA2^{D2723H} ES cells from S. Sharan (US National Institutes of Health) and sYFP cDNA from T. Gadella (University of Amsterdam). We thank D. Görlich (Max Planck Institute) for generously providing constructs encoding Ran^{Q69L} and CRM1 and for information concerning assay conditions. We thank members of the Venkitaraman laboratory for technical assistance and constructive discussions and M. Goode for help with the feeder-free culture for ES cell cultures. A.D.J. was supported by a career development fellowship from the UK MRC Cancer Unit. Work in the laboratory of C.F.K. was funded by the UK Biosciences and Biotechnology Research Council, and work in the laboratory of A.R.V. was funded by the UK MRC.

AUTHOR CONTRIBUTIONS

A.D.J. and A.R.V. conceived the project. Experiments were performed by A.D.J., A.B.J., J.S. and M.L. (microscopy); Y.L. and M.L. (biochemistry); and A.D.J., H.H., V.P., A.B.J., E.S., Y.R., K.S. and N.A. (cell biology). Structural analysis was performed by E.R., and FRET-FLIM analysis was performed by S.S. and C.F.K. A.D.J. and A.R.V. wrote the manuscript.

COMPETING FINANCIAL INTERESTS

The authors declare no competing financial interests.

1. The Breast Cancer Linkage Consortium. Cancer risks in BRCA2 mutation carriers. The Breast Cancer Linkage Consortium. *J. Natl. Cancer Inst.* **91**, 1310–1316 (1999).
2. Collins, N. *et al.* Consistent loss of the wild type allele in breast cancers from a family linked to the BRCA2 gene on chromosome 13q12–13. *Oncogene* **10**, 1673–1675 (1995).
3. King, T.A. *et al.* Heterogenic loss of the wild-type BRCA allele in human breast tumorigenesis. *Ann. Surg. Oncol.* **14**, 2510–2518 (2007).
4. Knudson, A.G. Jr. Mutation and cancer: statistical study of retinoblastoma. *Proc. Natl. Acad. Sci. USA* **68**, 820–823 (1971).
5. Skoulidis, F. *et al.* Germline Brca2 heterozygosity promotes Kras^{G12D}-driven carcinogenesis in a murine model of familial pancreatic cancer. *Cancer Cell* **18**, 499–509 (2010).
6. Xia, F. *et al.* Deficiency of human BRCA2 leads to impaired homologous recombination but maintains normal nonhomologous end joining. *Proc. Natl. Acad. Sci. USA* **98**, 8644–8649 (2001).
7. Moynahan, M.E., Pierce, A.J. & Jasin, M. BRCA2 is required for homology-directed repair of chromosomal breaks. *Mol. Cell* **7**, 263–272 (2001).
8. Chen, P.-L. *et al.* The BRC repeats in BRCA2 are critical for RAD51 binding and resistance to methyl methanesulfonate treatment. *Proc. Natl. Acad. Sci. USA* **95**, 5287–5292 (1998).
9. Yuan, S.S. *et al.* BRCA2 is required for ionizing radiation–induced assembly of Rad51 complex *in vivo*. *Cancer Res* **59**, 3547–3551 (1999).
10. Yang, H., Li, Q., Fan, J., Holloman, W.K. & Pavletich, N.P. The BRCA2 homologue Brh2 nucleates RAD51 filament formation at a dsDNA-ssDNA junction. *Nature* **433**, 653–657 (2005).
11. Thorslund, T. *et al.* The breast cancer tumor suppressor BRCA2 promotes the specific targeting of RAD51 to single-stranded DNA. *Nat. Struct. Mol. Biol.* **17**, 1263–1265 (2010).
12. Liu, J., Doty, T., Gibson, B. & Heyer, W.D. Human BRCA2 protein promotes RAD51 filament formation on RPA-covered single-stranded DNA. *Nat. Struct. Mol. Biol.* **17**, 1260–1262 (2010).
13. Jensen, R.B., Carreira, A. & Kowalczykowski, S.C. Purified human BRCA2 stimulates RAD51-mediated recombination. *Nature* **467**, 678–683 (2010).
14. Carreira, A. *et al.* The BRC repeats of BRCA2 modulate the DNA-binding selectivity of RAD51. *Cell* **136**, 1032–1043 (2009).
15. Shivji, M.K. *et al.* The BRC repeats of human BRCA2 differentially regulate RAD51 binding on single- versus double-stranded DNA to stimulate strand exchange. *Proc. Natl. Acad. Sci. USA* **106**, 13254–13259 (2009).
16. Goldgar, D.E. *et al.* Integrated evaluation of DNA sequence variants of unknown clinical significance: application to BRCA1 and BRCA2. *Am. J. Hum. Genet.* **75**, 535–544 (2004).

17. Karchin, R., Agarwal, M., Sali, A., Couch, F. & Beattie, M.S. Classifying variants of undetermined significance in BRCA2 with protein likelihood ratios. *Cancer Inform.* **6**, 203–216 (2008).
18. Marston, N.J. *et al.* Interaction between the product of the breast cancer susceptibility gene BRCA2 and DSS1, a protein functionally conserved from yeast to mammals. *Mol. Cell Biol.* **19**, 4633–4642 (1999).
19. Yang, H. *et al.* BRCA2 function in DNA binding and recombination from a BRCA2–DSS1-ssDNA structure. *Science* **297**, 1837–1848 (2002).
20. Kuznetsov, S.G., Liu, P. & Sharan, S.K. Mouse embryonic stem cell-based functional assay to evaluate mutations in BRCA2. *Nat. Med.* **14**, 875–881 (2008).
21. Zhou, Q. *et al.* Dss1 interaction with Brh2 as a regulatory mechanism for recombinational repair. *Mol. Cell Biol.* **27**, 2512–2526 (2007).
22. Jares-Erijman, E.A. & Jovin, T.M. FRET imaging. *Nat. Biotechnol.* **21**, 1387–1395 (2003).
23. Goedhart, J., Vermeer, J.E.M., Adjobo-Hermans, M.J.W., van Weeren, L. & Gadella, T.W.J. Jr. Sensitive detection of p65 homodimers using red-shifted and fluorescent protein-based FRET couples. *PLoS ONE* **2**, e1011 (2007).
24. Spain, B.H., Larson, C.J., Shihabuddin, L.S., Gage, F.H. & Verma, I.M. Truncated BRCA2 is cytoplasmic: implications for cancer-linked mutations. *Proc. Natl. Acad. Sci. USA* **96**, 13920–13925 (1999).
25. Wu, K. *et al.* Functional evaluation and cancer risk assessment of BRCA2 unclassified variants. *Cancer Res.* **65**, 417–426 (2005).
26. la Cour, T. *et al.* Analysis and prediction of leucine-rich nuclear export signals. *Protein Eng. Des. Sel.* **17**, 527–536 (2004).
27. Sonoda, E. *et al.* Rad51-deficient vertebrate cells accumulate chromosomal breaks prior to cell death. *EMBO J.* **17**, 598–608 (1998).
28. Pellegrini, L. *et al.* Insights into DNA recombination from the structure of a RAD51-BRCA2 complex. *Nature* **420**, 287–293 (2002).
29. Rajendra, E. & Venkitaraman, A.R. Two modules in the BRC repeats of BRCA2 mediate structural and functional interactions with the RAD51 recombinase. *Nucleic Acids Res.* **38**, 82–96 (2010).
30. Yu, D.S. *et al.* Dynamic control of Rad51 recombinase by self-association and interaction with BRCA2. *Mol. Cell* **12**, 1029–1041 (2003).
31. Rittinger, K. *et al.* Structural analysis of 14–3-3 phosphopeptide complexes identifies a dual role for the nuclear export signal of 14–3-3 in ligand binding. *Mol. Cell* **4**, 153–166 (1999).
32. Hantschel, O. *et al.* Structural basis for the cytoskeletal association of Bcr-Abl/c-Abl. *Mol. Cell* **19**, 461–473 (2005).
33. Güttler, T. *et al.* NES consensus redefined by structures of PKI-type and Rev-type nuclear export signals bound to CRM1. *Nat. Struct. Mol. Biol.* **17**, 1367–1376 (2010).
34. Davies, A.A. *et al.* Role of BRCA2 in control of the RAD51 recombination and DNA repair protein. *Mol. Cell* **7**, 273–282 (2001).
35. Xu, D., Farmer, A., Collett, G., Grishin, N.V. & Chook, Y.M. Sequence and structural analyses of nuclear export signals in the NESdb database. *Mol. Biol. Cell* **23**, 3677–3693 (2012).
36. Dong, X. *et al.* Structural basis for leucine-rich nuclear export signal recognition by CRM1. *Nature* **458**, 1136–1141 (2009).
37. Mladenov, E., Anachkova, B. & Tsaneva, I. Sub-nuclear localization of Rad51 in response to DNA damage. *Genes Cells* **11**, 513–524 (2006).
38. Gildemeister, O.S., Sage, J.M. & Knight, K.L. Cellular redistribution of Rad51 in response to DNA damage: a novel role for Rad51C. *J. Biol. Chem.* **284**, 31945–31952 (2009).
39. Ciccia, A. & Elledge, S.J. The DNA damage response: making it safe to play with knives. *Mol. Cell* **40**, 179–204 (2010).
40. San Filippo, J., Sung, P. & Klein, H. Mechanism of eukaryotic homologous recombination. *Annu. Rev. Biochem.* **77**, 229–257 (2008).
41. Dingwall, C. & Laskey, R.A. Protein import into the cell nucleus. *Annu. Rev. Cell Biol.* **2**, 367–390 (1986).
42. Krogan, N.J. *et al.* Proteasome involvement in the repair of DNA double-strand breaks. *Mol. Cell* **16**, 1027–1034 (2004).
43. Mannen, T., Andoh, T. & Tani, T. Dss1 associating with the proteasome functions in selective nuclear mRNA export in yeast. *Biochem. Biophys. Res. Commun.* **365**, 664–671 (2008).
44. Gudmundsdottir, K., Lord, C.J., Witt, E., Tutt, A.N. & Ashworth, A. DSS1 is required for RAD51 focus formation and genomic stability in mammalian cells. *EMBO Rep.* **5**, 989–993 (2004).
45. Saeki, H. *et al.* Suppression of the DNA repair defects of BRCA2-deficient cells with heterologous protein fusions. *Proc. Natl. Acad. Sci. USA* **103**, 8768–8773 (2006).
46. Edwards, S.L. *et al.* Resistance to therapy caused by intragenic deletion in BRCA2. *Nature* **451**, 1111–1115 (2008).
47. Sakai, W. *et al.* Secondary mutations as a mechanism of cisplatin resistance in BRCA2-mutated cancers. *Nature* **451**, 1116–1120 (2008).
48. Siaud, N. *et al.* Plasticity of BRCA2 function in homologous recombination: genetic interactions of the PALB2 and DNA binding domains. *PLoS Genet.* **7**, e1002409 (2011).
49. Kojic, M., Zhou, Q., Lisby, M. & Holloman, W.K. Brh2-Dss1 interplay enables properly controlled recombination in *Ustilago maydis*. *Mol. Cell Biol.* **25**, 2547–2557 (2005).
50. Han, X., Saito, H., Miki, Y. & Nakanishi, A.A. CRM1-mediated nuclear export signal governs cytoplasmic localization of BRCA2 and is essential for centrosomal localization of BRCA2. *Oncogene* **27**, 2969–2977 (2008).
51. Honrado, E. *et al.* Immunohistochemical expression of DNA repair proteins in familial breast cancer differentiate BRCA2-associated tumors. *J. Clin. Oncol.* **23**, 7503–7511 (2005).
52. Mitra, A. *et al.* Overexpression of RAD51 occurs in aggressive prostatic cancer. *Histopathology* **55**, 696–704 (2009).

ONLINE METHODS

Antibodies and siRNAs. The antibodies used in this work are listed in **Table 1**. The targeted mRNAs and the corresponding siRNA sequences used were *BRCA2* (Dharmacon siGenome),

1. GAAACGGACUUGCUAUUUA
2. GUAAAGAAAUGCAGAAUUC
3. GGUAUCAGAUGCUUCAUUA
4. GAAGAAUGCAGGUUUAAUA* (*also used as single siRNA);

BRCA2 (Qiagen, 5′ UTR), TTGGAGGAATATCGTAGGTAA;
CHK1 (Dharmacon siGenome),

1. GCAACAGUAUUUCGGUAUA
2. GGACUUCUCUCCAGUAAAC
3. AAAGAUAGAUGGUACAACA
4. CCACAUGUCCUGAUCAUAU;

ATM (Dharmacon siGenome),

1. GCAAAGCCCUAGUAACAUA
2. GGGCAUUACGGGUGUUGAA
3. UCGCUUAGCAGGAGGUGUA
4. UGAUGAAGAGAGACGGAAU;

ATR (Dharmacon siGenome),

1. GAACAACACUGCUGGUUUG
2. GCAACUCGCCUAACAGAUA
3. UCUCAGAAGUCAACCGAUU
4. GAAUUGUGUUGCAGAGCUU;

and *DSS1* (Eurofins MWG Operon),

1. GCAGCCGGUAGACUUAGGU
2. GAGUUCCCUGCCGAAGACU
3. UGUAGAGGAUGACUUCUCU
4. GAUGAAGAUGCACAUGUCU.

Plasmids and cloning. The BRCA2 DBD was cloned between 7382 and 8926 nt to generate fragments spanning residues 2461–2975 in hsBRCA2 using the following primers:

forward, 5′- AAGCCCAGAAAGGGTGCTTCTTCAAC;
reverse, 5′- GCACCCTTTCTGGGCTTAGGCATC.

These fragments were cloned into the vectors pEF-Myc-Nuc and pEGFP-C1-NotI (generated previously in our lab to contain an extra Not1 site in the multiple cloning site). The enhanced GFP (eGFP)-DBD plasmid was then digested to release the eGFP tag, which was replaced with an NLS-containing version of sYFP for nuclear localization using the following primers:

forward (including the NLS tag), 5′-GGCCGCTAGCATGGATCCAAAAAAG AAGAGAAAGGTAGATCCAAAAAAGAAGAGAAAGGTAGATCCAAAAAA GAAGAGAAAGGTAGTGAGCAAGGGCGAGGAGCTGTTCA-3′;
reverse, 5′- GAATCTCGAGTCTTGTACAGCTCGTCCATGCCGAGAGT- 3′ from the plasmid pSYFP2-C1 (a kind gift of T. Gadella, Amsterdam, The Netherlands).

The W2725A and D2723H mutations for disruption of DSS1 binding were introduced into these plasmids using the QuikChange mutagenesis kit (Stratagene) and the primers for NdeI-W2725A and NcoI-D2723H (5′- TTGA ACTTACAGATGGGGCATATGCTGTTAAGGCCCAGTTAG- 3′ and 5′- GCC ATTATTGAACTTACCCATGGGTGGTATGCTGTTAAGG- 3′, respectively).

Mutations were generated with the QuikChange XL site-directed mutagenesis kit (Stratagene) according to the manufacturer's instructions, with the exception that the digestion of the parental DNA template with DpnI was for 4 h.

The following primers were used in the cloning of the RAD51 nuclear exclusion signal:

RAD51 forward, GATCCAGGCAGATGCACTTGGCCAGGTTTCTGCGG ATGCTTCTGCGACTCGCTGATGAGTTTGGTTGAG;

reverse, AATTCTCAACCAAACTCATCAGCGAGTCGCAGAAGCATCCG CAGAAACCTGGCCAAGTGCATCTGCCTG.

pSYFP-C1 was digested with BglI and EcoRI before ligation with the annealed product of the RAD51 forward and reverse primers. The annealed primers spanned residues 241–260 of human RAD51 and resulted in in-frame fusion with sYFP.

The following primers were used in the cloning of the BRCA2 NES:

BRCA2 NES forward, GATCCGCAAAAACACTTGTTCTCTGTGTTTCT GACATAATTTCATTGAGCGCAAATATATGAG;

BRCA2 NES reverse, AATTCTCATATATTTGCGCTCAATGAAATTATGT CAGAAACACAGAGAACAAGTGTTTTTGCG;

BRCA2 control forward, GATCCGTTAAGGCCCAGTTAGATCCTCCCC TCTTAGCTGTCTTAAAGAATGGCAGACTGACAGTTGGTCAGTGAG;

BRCA2 control reverse, AATTCTCACTGACCAACTGTCAGTCTGCCATT CTTTAAGACAGCTAAGAGGGGAGGATCTAACTGGGCCTTAACG.

pSYFP-C1 was digested with BglI and EcoRI and ligated with the annealed product of the primers described above to yield the sYFP-NES and sYFP control sequences.

The pCAG-Flag-BRCA2–internal ribosome entry site (IRES)-Neo plasmid was generated in a two-step procedure. p3×Flag-BRCA2 (ref. 53) was modified by introducing an IRES fragment from the pIRES-Neo vector (Clontech) to generate Flag-tagged BRCA2 and a neomycin-resistant gene in a single transcript. Then the 3×Flag-BRCA2-IRES-Neo fragment was inserted to the pCAG-GFP vector (Addgene), and the early promoter regions of GFP and SV40 were removed to obtain the stable expression of the Flag-BRCA2 protein in SV40-transformed cells. The D2723H mutation was obtained using the QuikChange mutagenesis kit (Stratagene) and the primer (NcoI-D2723H)

5′-GCCATTATTGAACTTACCCATGGGTGGTATGCTGTTAAGG-3′.

To make the Flag-DSS1 construct, full-length (70 residues) DSS1 sequences were cloned into the HindIII and BamHI sites of the 3×Flag-CMV-10 vector (Sigma). The primers used were

forward, 5′-GTCAAGCTTTCAGAGAAAAAGCAGCCGGTAGAC-3′;
reverse, 5′-GGCGGATCCCTATGAAGTCTCCATCTTATAAC-3′.

Table 1 Antibodies used in this study

Antibody against[a]	Catalog or clone number	Source	Application	Dilution	Comments
RAD51	14B4	Genetex	WB	1:2,000	
RAD51	B01P	Abnova	IF	1:2,000	
RAD51	Ab1	Calbiochem	IF	1:1,000	Polyclonal serum (batches before 2010)
Flag tag	M2, F1804	Sigma	WB and IF	1:3,000 (WB), 1:2,000 (IF)	
DSS1 (goat polyclonal)	Ab5649	Abcam	WB and IF	1:1,000 (WB), 1:500 (IF)	
GFP	632381	Clontech	WB	1:2,000	
GFP	632381	Clontech	IP	1 µl per mg of lysate	Polyclonal serum, suitable only for IP
GFP	MBL-598	MBL	IF	1:1,000	
SCC1 (rabbit polyclonal)	Ab992	Abcam	WB	1:2,000	
MEK2	610236	BD Transduction Laboratories	WB	1:3,000	
BRCA2	Ab1, OP95	Merck	WB	1:500	Human BRCA2
BRCA2	H-300	Santa Cruz	WB	1:500	Pan-species
GST	AB92	Abcam	WB	1:5,000	
His tag	631212	Clontech	WB	1:5,000	

WB, western blotting; IF, immunofluorescence; IP, immunoprecipitation.

[a]The proteins to which the antibodies are specific are listed.

To make the mCherry-DSS1 construct, full-length DSS1 sequences were cloned between the BstB1 and BamHI sites, which excised RAD51 from a previously described[54] mCherry-RAD51 vector. The primers used were

forward, 5′-GCGTTCGAATATGTCAGAGAAAAAGCAGCCGGTAG-3′;

reverse, 5′-CGCGGATCCCTATGAAGTCTCCATCTTATAAC-3′.

To make the sYFP-RAD51 and sYFP-RAD51-SA-ED constructs, full-length sYFP sequences (from pSYFP-C1) were cloned into AgeI and SacI sites, which excised eGFP from eGFP-RAD51 and eGFP-RAD51-SA-ED (previously described in ref. 30). The primers used were

forward, 5′-ATACCGGTATGGTGAGCAAGGGCGAGGAGCTGTT-3′;

reverse, 5′-ATGAGCTCGCTTGTACAGCTCGTCCATGCCGAGAGT-3′.

To make the GST-DBD construct for the *in vitro* binding assay, the BRCA2 DBD (from hsBRCA2 residues 2461–2975) was PCR amplified from the NLS-sYFP-DBD construct and cloned into the SalI and NotI sites of the vector pGEX-4T3 (GE Healthcare). For GST-DBD^{D2723H}, the same region was PCR amplified from the NLS-sYFP-DBD^{D2723H} construct. The primers used were

forward, 5′-GCGTCGACAACTCCAATCAAGCAGCAGCT-3′;

reverse, 5′-GCGCGGCCGCTCATACAATACGCAACTTCCACAC-3′.

To make the GST-RAD51^{F86E} and GST-RAD51-SAM constructs, the respective RAD51 mutant sequences were PCR amplified from the GFP-RAD51^{F86E} and GFP-RAD51-SAM constructs[30] and cloned into the SalI and NotI sites of the vector pGEX-4T3 using the following primers:

forward, 5′-GCGTCGACATGGCAATGCAGATGCAGCTT-3′;

reverse, 5′-GCGCGGCCGCTCAGTCTTTGGCATCTCCCACT-3′.

To make the His-DSS1 construct, full-length DSS1 sequences were cloned into the NdeI and BamHI sites of a modified pET28a vector (Novagen). The primers used were

forward, 5′-GCGCCATATGTCAGAGAAAAAGCAGCCG-3′;

reverse, 5′-GCGCGGATCCCTATGAAGTCTCCATCTTATAACC-3′.

The CRM1 and Ran^{Q69L} constructs for bacterial overexpression were gifts from D. Görlich[33,55] (Max Planck Institute, Gottingen). BRC4 peptides were synthesized by Cambridge Research Biochemicals Ltd. with an N-terminal biotin moiety attached through a six–aminohexanoic acid spacer and a C-terminal amide. The sequence of the peptide was KEPTLLGFHTASGKKVKIAKESLD KVKNLFDEKEQ.

Cell culture and transfection. 293T and U2OS cells were cultured in sterile filtered growth medium (DMEM with GlutaMAX-1, 4,500 mg l^{-1} D-glucose, sodium pyruvate and pyridoxine (Gibco) supplemented with 10% fetal calf serum (Gibco) and 2% penicillin-streptomycin (Gibco)) in a 37 °C humidified incubator in the presence of 5% CO_2. Cells were split every 2–3 d and maintained at 50% confluency. MCF10A cells were grown in DMEM and F12 (1:1) with 15 mM HEPES (Gibco) supplemented with 5% horse serum (Invitrogen), 10 μg ml^{-1} insulin (Sigma), 20 ng ml^{-1} epidermal growth factor (Sigma), 100 ng ml^{-1} cholera toxin (Sigma), 500 ng ml^{-1} hydrocortisone (Sigma) and 1% penicillin-streptomycin. ES cells were grown in gelatinized plates with Glasgow minimum essential medium (Sigma) supplemented with 15% FBS (Hyclone), 1 mM sodium pyruvate, 1× nonessential amino acids (Invitrogen), 1× glutamate-penicillin-streptomycin, (Invitrogen), 100 μM β-mercaptoethanol and 1,000 units per ml of leukemia inhibitory factor (ESGRO Chemicon).

Transient transfection of DBD plasmids was performed by lipofection using Lipofectamine 2000 (Invitrogen) using 1 μg DNA and 3 μl Lipofectamine in OptiMEM (Invitrogen) for 10^6 cells. For high-content microscopy, U2OS cells were plated in a 24-well plate. 1 d after plating, cells were transfected with a NLS-sYFP-DBD construct (either WT or the D2723H mutant; 0.25 μg) together with an empty mCherry plasmid or an mCherry-DSS1 plasmid (0.125 μg) using Lipofectamine. Full-length BRCA2 was introduced into U2OS cells using the Amaxa Cell Line Nucleofector Kit V and the Nucleofector I device with the program X-01 (Lonza). For high-content microscopy experiments, MCF10A cells were reverse transfected with the indicated siRNAs at a final concentration of 25 nM using Dharmafect I transfection reagent (Fermentas GmbH, Thermo Fisher Scientific) in a 96-well plate. EUFA423BRCA2 (EUFA-BRCA2#34) cell lines were established by stably transfecting EUFA423 cells (SV40-immortalized BRCA2-deficient human fibroblasts) with the pCAG-Flag-BRCA2-IRES-Neo construct in standard DMEM plus 10% FBS with penicillin-streptomycin supplemented with 750 μg ml^{-1} G418.

Cell viability assay. Cells were plated into 96-well plates at a density of 8,000 cells per well. Different doses of MMC (Sigma) were added (four wells per dose per cell line), and the plates were incubated at 37 °C for five doubling times. CellTiter-Blue reagents (Promega) were added to each well of the 96-well plate according to the manufacturer's guidelines. The plates were incubated at 37 °C for ~1–2 h in a humidified 5% CO_2 atmosphere. The number of viable cells was determined using the Fusion plate reader at an absorbance of 590 nm. A similar procedure was followed for the cell viability assay for ES cells exposed to different doses of ionizing radiation using a Faxitron X-ray unit.

Lifetime measurements. DBD- and DSS1-transfected cells were plated on MatTek poly-D-lysine–coated, number 1 glass-bottomed 35-mm dishes, and the medium was replaced with phenol red–free L15. Experiments were performed on a TCSPC system (Becker and Hickl Inc., SPC 830) connected to the descanned and fiber-coupled output of an Olympus FV300 confocal scanner (Laser Analytics Group, Department of Chemical Engineering). A supercontinuum laser (Fianium Inc., SC400) was used as the illumination source. An excitation wavelength of 436 ± 1 nm (range) was selected by an Acousto Optic Tunable Filter (AOTFnC VIS, AA Opto-Electronique, Orsay, France) and coupled into the confocal scanner. The fluorescence output was filtered between 480 and 550 nm before being detected by the TCSPC photomultiplier tube. TCSPC data were analyzed to generate lifetime information on dedicated Matlab (MathWorks, Inc.) and Becker and Hickl software.

Immunofluorescence analyses. Cell staining and immunofluorescence analyses were carried out as described previously[56]. Briefly, transfected and untransfected cells were grown on coverslips and subjected to different treatments as indicated in the text before fixation. Cells for IF experiments were grown on coverslips to 70–80% confluence, washed in PBS and fixed in 4% paraformaldehyde or 95% ethanol plus 5% acetic acid. The cells were permeabilized by adding Tris-buffered saline (TBS) with 0.1% Triton X-100 and 0.2% Tween (TBS-Triton-Tween) for 5 min, blocked in TBS-Triton-Tween plus 2% BSA and incubated with the indicated primary and secondary antibodies (**Table 1**) in a humidified chamber with TBS-Tween-Triton washes between the primary and secondary incubation. The coverslip was then mounted onto a slide for viewing using a mounting medium with DAPI. Immunofluorescence images were captured using a Zeiss Axiovert200 LSM510meta confocal microscope using a 40× objective with fixed optical slice, laser power and detector and amplifier settings for all samples across each individual experiment to allow for comparison.

High-content microscopy for adherent cells. High-content microscopy experiments were performed on the Cellomics VTI-Arrayscan Instrument (Thermo Fisher), as described previously[56], in 96-well (Nunc) or 24-well plates. Transfections were performed using 0.25 μg or 0.125 μg of DNA and Lipofectamine. The cells were treated with specified DNA-damaging agents, fixed with 4% formaldehyde for 10 min, immunostained as per conventional protocols and incubated with 0.1% Triton X-100 with Hoechst 33342 DNA dye for 10 min followed by PBS washes. Cellomics VTI ArrayScan was used for image acquisition using the Compartmental Analysis BioApplication and a 40× nonimmersion objective. Hoechst staining was used for object identification, and the average intensity of the fluorescent signal per nucleus was estimated using the target-activation Cellomics BioApplication. 300–500 cells were analyzed per well, and standard errors were calculated from an average of the means of multiple wells.

Immunoprecipitation. Whole-cell extracts were prepared from 15 × 10^6 293T cells 24 h after transfection. The trypsinized or scraped cells were spun down in a Beckman centrifuge at 1,000 r.p.m. for 3 min, washed once with PBS and resuspended in 1 ml of ice-cold immunoprecipitation lysis buffer (50 mM HEPES, pH 7.4, 100 mM NaCl, 0.5% NP-40, 10 mM EDTA, 2 mM β-glycerophosphate, 1 mM DTT and 1 mM PMSF supplemented with protease inhibitors (Roche)) for 15 min on ice. Extracts were then spun down in an Eppendorf centrifuge for 15 min at 12,000 r.p.m., and the supernatant was collected and quantified for protein concentration by the bicinchoninic acid assay (Sigma). 1 mg of whole-cell extract was precleared with 30 μl of a 50% slurry of protein A–Sepharose (Sigma) for 20 min at 4 °C with gentle shaking to reduce nonspecific protein-bead interactions followed by immunoprecipitation using 1–2 μg of antibody

doi:10.1038/nsmb.2666

(specified in **Table 1**) and 30 µl of a 50% slurry of protein A–Sepharose overnight in a cold room with gentle shaking. The immune complexes were then washed four times in ice-cold immunoprecipitation lysis buffer and one time in PBS before resuspension in 4× loading buffer (Invitrogen) and 50 mM DTT.

***In vitro* pulldown assays.** The *in vitro* CRM1 binding assays were performed using an assay described previously[33]. For each assay condition, 1 µg of GST-tagged protein (DBD, DBD^{D2723H}, RAD51^{F86E} or RAD51-SAM) bound to glutathione–Sepharose 4B beads was incubated with 1 µM CRM1 and/or Ran-GTP, as indicated, for 1 h at 4 °C in 500 µl of binding buffer (50 mM HEPES, pH 7.5, 150 mM NaCl, 25 mM KCl, 50 mM LiCl, 2 mM $Mg(OAc)_2$, 5 mM DTT and 20 µM GTP-γS (a nonhydrolyzable GTP analog)). DSS1 proteins or BRC4 peptides (or binding buffer alone for the GST control) were then added to individual tubes as indicated, followed by incubation at 4 °C for 2 h. Beads were washed three times with 500 µl of binding buffer, followed by elution of proteins and SDS-PAGE. DBD, DBD^{D2723H}, RAD51^{F86E} and RAD51-SAM were detected by immunoblotting with antibody to GST (**Table 1**), and CRM1 was detected by immunoblotting with His-specific antibody (**Table 1**).

Cell fractionation. Cells were washed in PBS and resuspended in solution A (10 mM HEPES, pH 7.9, 10 mM KCl, 1.5 mM $MgCl_2$, 0.34 M sucrose, 10% glycerol, 1 mM DTT, protease and phosphatase inhibitors). Cells were incubated on ice for 5 min, and the cytoplasmic (S1) and nuclear (P1) fractions were harvested by centrifugation at 1,300*g* for 4 min. Isolated nuclei were then washed in solution A, lysed in solution B (0.1% Triton X-100, 3 mM EDTA, 0.2 mM EGTA, 1 mM DTT, protease and phosphatase inhibitors) and incubated on ice for 10 min. The soluble nuclear (S3) and chromatin fractions were harvested by centrifugation at 1,700*g* for 4 min. To release chromatin-bound proteins by nuclease treatment, the P2 fraction was incubated in solution A plus 1 mM $CaCl_2$ and 5 U micrococcal nuclease for 15 min at 37 °C, after which the reaction was stopped by the addition of 1 mM EGTA and spun down at 10,000*g* to collect the supernatant enriched for chromatin proteins (P3). The S3 and P3 fractions were pooled to obtain a nuclear extract.

Proteins were resolved on 3–8% Tris-acetate SDS-PAGE (Invitrogen) for the BRCA2 experiments, 4–12% MES SDS-PAGE (Invitrogen) for most of the other experiments and 4–20% Tris-glycine gels for the DSS1 experiments. Transfer was performed to PVDF membranes (Immobilon-P, Millipore) at 30 V for 2 h. Western blots were blocked in 5% milk (Marvel) and 0.5% Tween-20 in TBS for 30 min at room temperature before probing with the appropriate primary antibodies (**Table 1**). Western blots were developed with horseradish peroxidase–conjugated secondary antibodies against rabbit and mouse at 1/1,5000 and 1/1,0000, respectively, and detected with either enhanced chemiluminescence (ECL) or ECL Plus detection reagents (Amersham) and exposed to CL-Xposure Film (Pierce).

Quantitative RT-PCR. To analyze the effects of siRNA knockdown, 0.5 µg of total RNA, which was extracted with the RNeasy Plus Mini Kit (Qiagen), was used for cDNA synthesis using the Cloned AMV First-Strand Synthesis kit (Invitrogen). Quantitative RT-PCR was performed using the LightCycler 480 SYBR Green I Master mix (Roche) with the following primers:

GAPDH forward, TGAGCTTGACAAAGTGGTCG; reverse, GTCAGTGGT GGACCTGACCT;

CHK1 forward, CCAGATGCTCAGAGATTCTTCCA; reverse, TGTTCA ACAAACGCTCACGATTA;

ATM forward, GGCTATTCAGTGTGCGAGACA; reverse, TGGCTCC TTTCGGATGATGGA;

ATR forward, TCCCTTGAATACAGTGGCCTA; reverse, TCCTTGA AAGTACGGCAGTTC;

DSS1 forward, GAAAAAGCAGCCGGTAGACTT; reverse, ATCCCAAT TATCCTCCCAGACA;

BRCA2 forward, TTGGCTGATGGTGGATGGCTCATA; reverse, TTTGGA TCCACACCTGGAGTGTCA.

The cycle threshold (Ct) values were obtained from the LightCycler 480 and referenced to the expression of the housekeeping gene, *GAPDH*. All samples were then normalized to the non-Targeting siRNA pool (Fermentas GmbH).

For the RT-PCR comparison between mm*Brca2* and hs*BRCA2*, the following primers were used:

mouse GAPDH forward, GAAGGTCGGTGTGAACGGATTT; reverse, CATTTGATGTTAGTGGGGTCTC;

Brca2 5022F, TTATGCAGGAATCTTTGGACA; 5173R, AGTTCTGC ATTTCTTCACATTTT;

BRCA2 731F, AAAGTTTGTGAAGGGTCGTC; 840R, TAAGGGTGGG TGGTGTAGC.

RNA was made from exponentially growing ES cells using a Qiagen total RNA kit. 2 µg RNA was converted into cDNA using the Roche Transcriptor High Fidelity cDNA Synthesis Kit, and quantitative RT-PCR was performed as described above. The Ct values were directly represented in the figure to provide an unbiased assessment, and GAPDH was used as a control.

The original images of the blots presented in this study are shown in **Supplementary Figure 8**.

53. Hattori, H., Skoulidis, F., Russell, P. & Venkitaraman, A.R. Context dependence of checkpoint kinase 1 as a therapeutic target for pancreatic cancers deficient in the BRCA2 tumor suppressor. *Mol. Cancer Ther.* **10**, 670–678 (2011).
54. Jeyasekharan, A.D. *et al.* DNA damage regulates the mobility of Brca2 within the nucleoplasm of living cells. *Proc. Natl. Acad. Sci. USA* **107**, 21937–21942 (2010).
55. Frey, S., Richter, R.P. & Gorlich, D. FG-rich repeats of nuclear pore proteins form a three-dimensional meshwork with hydrogel-like properties. *Science* **314**, 815–817 (2006).
56. Ayoub, N., Jeyasekharan, A.D., Bernal, J.A. & Venkitaraman, A.R. HP1-β mobilization promotes chromatin changes that initiate the DNA damage response. *Nature* **453**, 682–686 (2008).